J. Fluid Mech. (2010), *vol.* 648, *pp.* 183–203.
doi:10.1017/S0022112009993041

On properties of fluid turbulence along streamlines

LIPO WANG†

Institut für Technische Verbrennung, RWTH-Aachen, 52056 Aachen, Germany

(Received 20 February 2009; revised 23 October 2009; accepted 23 October 2009)

Geometrical and dynamical properties of turbulent flows have been investigated by streamline segment analysis. Starting from each grid point, a streamline segment is defined as the part of its streamline bounded by the two adjacent extremal points of the velocity magnitude. Physically the streamline segments can be extended into a more meaningful concept, namely the streamtube segments, which are non-overlapping and space filling. This decomposition of the flow allows for new insights into vector-related statistics in turbulence. According to the variation of velocity, the streamline segments can be sorted into positive and negative segments. The overall properties of turbulent flows can be newly understood and explained from the statistics of these segments with simple structures; for instance, the negative skewness of the velocity derivative becomes naturally a kinematic outcome. Furthermore, from direct numerical simulations conditional statistics of pressure and kinetic energy dissipation along the streamline segments are evaluated and discussed.

1. Introduction

The objective of the present paper is to address the spatial properties of turbulent fields based on a new method named streamline analysis. Although it can be described by the deterministic Navier–Stokes equations, turbulence is by no means temporally and spatially deterministic. It has been recognized that turbulent flows have both organized and disorganized parts (Lumley & Yaglom 2001). The randomness of turbulence is mainly from the disorganized part, while the organized part can manifest itself from correlations among some parameters of interest over a range of space and/or time that is significantly larger than the smallest local scales of the flow (Robinson 1991). To address the organized motions, it is more meaningful to understand the non-local statistics instead of local statistics. In the history of turbulence study the well-known theories on non-locality are the two-point Kármán–Howarth correlation equation and the structure function by Kolmogorov. However, for a deeper insight into the spatial dynamics of turbulence, there is a strong need to extend these classical statistical tools that focus on single or finite number of points into fieldwise or spatial topologies.

Remarkable progresses in understanding the spatial structures of turbulent flows have been made possible because of the use of flow visualization, based on both experimental and numerical data. In the last decades, one of the greatest achievements

† Present address: UM-SJTU Joint Institute, ShangHai JiaoTong University, 800 Dong Chuan Road, 200240 Shanghai, China. Email address for correspondence: wang@itv.rwth-aachen.de

from visualization is the understanding of vortex structures and intermittency (She, Jackson & Orszag 1990; Moffatt, Kida & Ohkitain 1994; Kaneda & Ishihara 2006). The regions of intense vorticity usually exist as tubes, named vortex tubes (She *et al.* 1990). In many respects, vortex tubes are believed to be important for organized motions and intermittency of turbulence. Moffatt *et al.* (1994) described vortex tubes as the 'sinews' of turbulence because of their important role in energy dissipation. On average, vortex tubes have radii of the Kolmogorov scale η, while it is generally believed that the tube length is comparable to the Taylor microscale or other smaller scales (Kaneda 2009, private communication). Compared with the pointwise statistics, the spatial field structures in the vicinity of vortex tubes are more meaningful in understanding turbulence. Along this direction, in the noticeable work by Synge & Lin (1943) and Aivazis & Pullin (2001), each vortex tube was idealized as a simple Hill's spherical vortex, and by averaging all the tubes over unbiased orientations (assumption), they derived the velocity structure functions with good agreement with experimental results. Other work, for example on critical points by Perry & Chong (1987) and stagnation points by Davila & Vassilicos (2003), may also indicate the footprint of spatial field motions in turbulence.

Although the knowledge of local geometric objects, such as vortex tubes and critical points, is a step forward in addressing turbulent structures, there are enough reasons to extend further the state of the art. Specifically, vortex tubes take only a small portion of the flow volume and thus are not complete to represent the overall properties of the entire fields. It may also be argued that the overall properties can be bridged from local statistics by turbulence modelling, which, however, is by no means satisfactory and convincing, at least from the fundamental point of view. Hamman, Klewicki & Kirby (2008) asserted that there are some advantages of connecting directly the attributes of organized motions to field variables, for instance the divergence of the Lamb vector, because of its high impact on the changing rate of momentum. Some other field variables may also serve similar purposes. Moffatt & Tsinober (1992) discussed the effect of helicity density on turbulent dynamo and applied this parameter for characterizing complex three-dimensional flows, for example the relation between helicity and vortex breakup.

In recent years, a novel idea to investigate the turbulent structures is to decompose the original flow field into dissipation elements (Wang & Peters 2008, 2006). In a given snapshot of the scalar field, starting from every grid point, a trajectory along the ascending and descending gradients can be traced until it reaches local maximum and minimum points, respectively. A dissipation element is defined as the spatial region containing all the grid points whose trajectories can share the same pair of maximal and minimal points. This decomposition is non-arbitrary and space filling, which thus uniquely makes possible the quantitative analyses of the entire field. Compared with the original entire field, dissipation elements have much simpler structures, and therefore they are easier to be well described by a set of parameters $(p_1, p_2, \ldots)$. Theoretically the joint probability density function (p.d.f.) $P(p_1, p_2, \ldots)$ plays a central role in relevant studies. From the viewpoint of turbulence modelling, it is hopeful to expect that a statistical property X may better be related to p_i in these relatively simple decomposed units than in the entire fields. Supposing $X = X(p_1, \ldots, p_n)$, the mean value $\langle X \rangle$ is

$$\langle X \rangle = \int \ldots \int X(p_1, \ldots, p_n) P(p_1, \ldots, p_n)\, \mathrm{d}p_1 \ldots \mathrm{d}p_n. \tag{1.1}$$

Moreover, various marginal p.d.f.s can also be obtained from the joint p.d.f.

This method works successfully on the passive scalar (Wang & Peters 2006) and other scalar field variables (Wang & Peters 2008; Mellado, Wang & Peters 2009) with important applications. However, it is not satisfactory to apply the same idea to the vector fields, which are topologically different from the scalar fields. Therefore a different approach is needed to depict the velocity vector in a 'natural' way to apply (1.1) to vector problems, as the gradient trajectory for scalars. In this context, streamlines can be a meaningful candidate to attack this difficulty.

The concept of streamlines comes naturally out of vector analysis in fluid mechanics. Actually a similar idea can be applied to other vector fields as well, such as magnetic lines and trajectories in phase space. Streamlines are the imaginary lines whose tangents indicate the direction of the fluid velocity. Steady flows have spatial constant streamlines, while for unsteady flows, streamlines change continuously, according to the variation of velocity. For Eulerian flows, along the same streamline Bernoulli's equation holds.

In principle, both gradient trajectories and streamlines are the natural topologies for the scalar and vector fields, respectively; however, in turbulence, usually gradient trajectories are of finite lengths, while streamlines may be infinitely long, unless they hit stagnation points with zero velocity. Stagnation points are of particular interest in analysing the change of patterns of streamlines. Davey (1961) and Lighthill (1963) considered flow separation and also streamline separation for the boundary layer problem. Rao (1978) pointed out that the main parameters characterizing streamlines and the effect on flowing are the curvature and the torsion, which are implicit functions involved with the velocity magnitude. Brons (2007) discussed the bifurcation patterns of streamlines systematically in a two-dimensional space, and the idea can also be applied to higher-dimensional problems. For two-dimensional flows, if not degenerated, there are two types of the streamline topology around stagnation points: one is spiral, and the other is saddle. The degenerated cases are more complicated. The work by Yannacopoulos, Rowlands & King (2002) provided a criteria for the breakup of a closed streamline.

Most streamlines are not bounded, except for those attached to stagnation points. Thus the general idea, (1.1) as in dissipation element analysis, cannot directly be applied to vector studies. To overcome this difficulty, one of the central tasks in the current paper is to study some intrinsic structures, based on which the velocity vector fields can be partitioned in an unbiased and space filling manner. In addition, as mentioned before, most discussions in the literature on streamlines are about the geometrical topologies. In many respects, it is more important and meaningful to investigate the kinematical and dynamical behaviours, which, however, is still scarce. It is evident that along streamlines velocity behaves as a one-dimensional scalar, which then can hopefully simplify the problems or, at least, assume the difficulty in a different manner.

This paper is organized according to the following issues:

(i) How will the basic fluid dynamics equations appear in the streamline frame? Comparatively, how are the new presentations different from and related to the conventional counterparts in the Cartesian coordinate system? How will the geometrical properties of streamlines play their roles in turbulent flows?

(ii) By which means from streamline analysis can turbulent flows be space filling, partitioned in a natural way? Will it be helpful to understand the finer structures of turbulence from this spatial partition?

(iii) Statistically how will these partitioned units behave and how are their structures to be described quantitatively? In what manner can the overall properties be

understood and explained by the knowledge of the relatively simple partitioned units?

2. Presentation of basic equations in the streamline frame

As pointed out by Hamman *et al.* (2008), the heart of the challenge to investigate organized motions is the lack of rigorous equations to describe the dynamics. In this section, we will tentatively present the basic fluid dynamics equations along streamlines, based on which further analyses may quantitatively be implemented.

In opposition to the commonly used Lagrangian viewpoint, which focuses on spatial moving particles in a continuous time span, the following analyses pertain only to snapshots of the flows, i.e. the entire flow fields at individual frozen moments. The overall statistics can be represented by the results from those snapshots if the Reynolds number is large enough.

2.1. *Mass balance and extremal surface*

Along a streamline the velocity vector is $\boldsymbol{v} = u\boldsymbol{t}$, where u is the magnitude and $\boldsymbol{t} = \boldsymbol{v}/|\boldsymbol{v}|$ is the unit orientation vector (except for stagnation points). To build a coordinate transform correspondence between the conventional Cartesian system and the streamline frame, besides the vector $\boldsymbol{t}$, other two orthogonal directions $\boldsymbol{n}$ and $\boldsymbol{b}$ (for three-dimensional problem) in compliance with the right-hand convention are also needed. Compared with the Cartesian system, the orientation vectors $(\boldsymbol{t}, \boldsymbol{n}, \boldsymbol{b})$ are non-constant but space and time dependent.

For incompressible flows, mass conservation is given by

$$\nabla \cdot \boldsymbol{v} = \nabla \cdot (u\boldsymbol{t}) = u\nabla \cdot (\boldsymbol{t}) + \boldsymbol{t} \cdot \nabla u = 0, \tag{2.1}$$

which can further be written as

$$u\kappa + \frac{\partial u}{\partial s} = 0, \tag{2.2}$$

where s is the curvilinear coordinate along streamlines; $\partial/\partial s = \boldsymbol{t}\cdot\nabla$; and the curvature κ is defined as $\kappa = \nabla \cdot \boldsymbol{t}$. The geometrical meaning of κ is the Gaussian curvature of the surfaces 'normal' to streamlines. Introducing the three Lame coefficients h_1, h_2 and h_3 in the $\boldsymbol{t}$, $\boldsymbol{n}$ and $\boldsymbol{b}$ directions, respectively, and for convenience setting $h_1 = 1$, κ can be expressed as $\kappa = (1/(h_2(s)h_3(s)))(\partial(h_2(s)h_3(s)))/\partial s$. Equation (2.2) shows that the Gaussian curvature κ is related to u and $\partial u/\partial s$ by

$$\kappa = -\frac{1}{u}\frac{\partial u}{\partial s}. \tag{2.3}$$

Equation (2.3) is a representation of mass conservation in terms of the geometrical parameter κ. Specially for extremal points of u or extremal points for simplicity, i.e. the points satisfying $\partial u/\partial s = 0$, some interesting consequences can be drawn. First we will demonstrate that streamlines at extremal points must locally be parallel. As shown in figure 1, for any streamline (solid ones) one can plot its streamtube (dashed boundaries consisting of an ensemble of streamlines and thus not unique). Because of mass conservation, the velocity magnitude u and the area A of the cross-surface, which is locally normal to streamlines, satisfy the following relation:

$$uA = \text{constant}. \tag{2.4}$$

Therefore the cross-area A can reach its local extremal A_E only at some extremal point E, where streamlines must be parallel, while at a non-extremal point P, streamlines

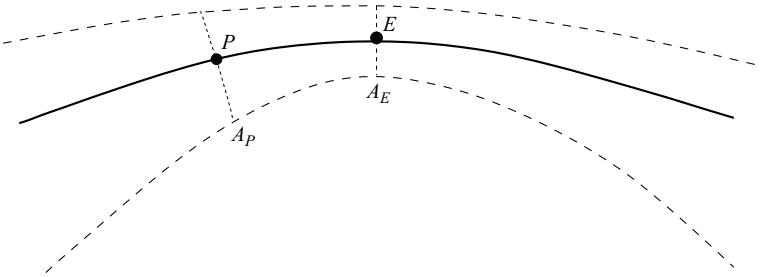

FIGURE 1. For viscous flows without velocity slipping, because of mass conservation, the cross-area A can reach its extremal A_E only at the extremal point E, and streamlines thereby must be parallel. Inversely any point on A_E should be the extremal point with respect to the streamline passing through; therefore extremal surfaces are cross-surfaces. For a non-extremal point P, streamlines need not to be parallel.

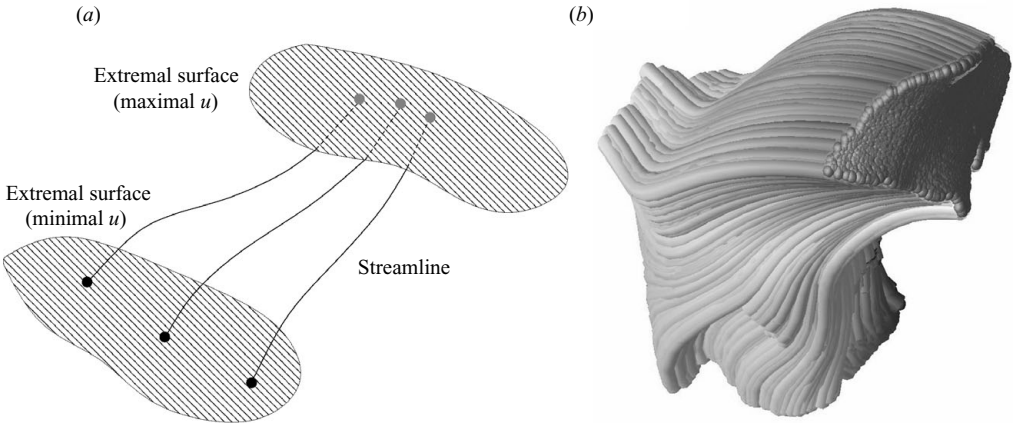

FIGURE 2. (*a*) Illustration of three-dimensional extremal surfaces (grey points for maximum and dark point for minimum). Because of mass conservation, from local minimal u to local maximal u the cross-area shrinks. (*b*) A DNS result showing the zero Gaussian curvature of a maximal surface, where the tubes represent streamlines and the colour is for the velocity magnitude.

around are not parallel. Further we can conclude that any point on A_E is an extremal point with respect to the streamline passing through it. Thus extremal surfaces are cross-surfaces, and from (2.3) we obtain that for extremal surfaces

$$\kappa = 0 \quad \text{for} \quad u \neq 0. \tag{2.5}$$

In the following for convenience, surfaces consisting of extremal points will be defined as extremal surfaces and, more specifically, as minimum-point or maximum-point surfaces, for minimal u or maximal u, respectively. The physical implication of (2.3) is that for streamlines with increasing u ($\partial u/\partial s > 0$) or decreasing u ($\partial u/\partial s < 0$), the cross-surfaces have negative and positive Gaussian curvatures, respectively. Only at extremal surfaces the Gaussian curvature is zero; therefore they are minimal surfaces.

Figure 2(*a*) illustrates schematically the case in three-dimensional space. Because of mass conservation, the cross-area decreases along streamline from a minimum-point surface to a maximum-point surface and vice versa. Figure 2(*b*) shows the numerical result from direct numerical simulation (DNS), where a bundle of streamlines stop

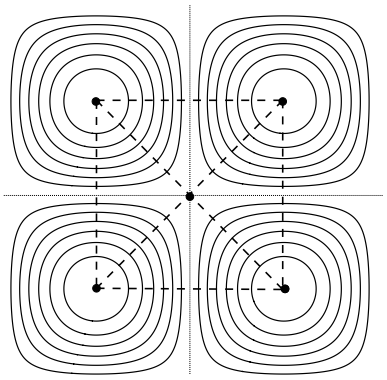

FIGURE 3. Illustration of extremal surfaces in two-dimensional space for the Taylor–Green vortex array. The four square-shaped dashed lines are the maximum-point lines, and the two dashed diagonal lines are the minimum-point lines. These extremal lines cross only at stagnation points because of singularity.

at their respective maximum points to form an extremal surface with zero Gaussian curvature.

Specially for the two-dimensional case, extremal surfaces with zero Gaussian curvature degenerate into straight lines. This picture can be better understood from a typical example, namely the Taylor–Green vortices. As shown in figure 3, the solid circles represent streamlines, and the dashed lines are extremal surfaces for this vortex array. Specifically, the four square-shaped dashed lines are the maximum-point lines, and the two diagonal ones are the minimum-point lines. Equation (2.5) shows that the zero Gaussian curvature is valid at non-stagnation points ($u \neq 0$). For stagnation points with $u = 0$, (2.3) suggests that κ is undetermined at this singularity, which corresponds to the crossing of extremal surfaces. In conclusion, extremal surfaces in two-dimensional space may change directions or cross with each other only at stagnation points.

2.2. *Momentum balance*

The momentum (Navier–Stokes) equations of incompressible fluids in vector form are

$$\frac{\partial \boldsymbol{v}}{\partial t} + \boldsymbol{v} \cdot \nabla \boldsymbol{v} = -\frac{1}{\rho}\nabla p + \nu \nabla \cdot \nabla \boldsymbol{v}, \tag{2.6}$$

where $\boldsymbol{v}$, p and ν are the velocity vector, pressure and kinematic viscosity, respectively.

Dot-multiplying the both sides of (2.6) with $\boldsymbol{t}$, $\boldsymbol{t}\cdot\partial\boldsymbol{v}/\partial t = \partial u/\partial t$ because $\boldsymbol{t}\cdot\partial\boldsymbol{t}/\partial t = 0$. The convection term in (2.6) can be written as $\boldsymbol{v}\cdot\nabla\boldsymbol{v} = u\partial\boldsymbol{v}/\partial s$, where s is the arclength coordinate along streamlines. Thus the equation for the velocity magnitude u is given by

$$\frac{\partial u}{\partial t} + u\frac{\partial u}{\partial s} = -\frac{1}{\rho}\frac{\partial p}{\partial s} + \underbrace{\nu \boldsymbol{t} \cdot (\nabla \cdot \nabla \boldsymbol{v})}\, A, \tag{2.7}$$

in which the viscous part A is

$$A = \nu \boldsymbol{t} \cdot [\nabla \cdot (\nabla u \otimes \boldsymbol{t} + u \nabla \boldsymbol{t})] = \nu \boldsymbol{t} \cdot [2\nabla u \cdot \nabla \boldsymbol{t} + \nabla^2 u \boldsymbol{t} + u \nabla \cdot \nabla \boldsymbol{t}] = \nu[\nabla^2 u + uG], \tag{2.8}$$

where

$$G \equiv \boldsymbol{t} \cdot (\nabla \cdot \nabla \boldsymbol{t}) = t_j \frac{\partial}{\partial x_i}\left(\frac{\partial t_j}{\partial x_i}\right) = -\frac{\partial t_j}{\partial x_i}\frac{\partial t_j}{\partial x_i}. \tag{2.9}$$

This parameter G can be understood as the shape factor of streamlines because it is implicitly determined by the spatial topology, such as the curvature and the torsion. Systematically G can be expressed in terms of the Lame coefficients h_1, h_2 and h_3 (see, e.g., the methods by Petrila & Trif 2005). Finally the momentum equation for u along streamlines is

$$\underbrace{\frac{\partial u}{\partial t}}_{LA} + \underbrace{u\frac{\partial u}{\partial s}}_{CV} = \underbrace{-\frac{1}{\rho}\frac{\partial p}{\partial s}}_{PG} + \underbrace{\nu\nabla^2 u}_{V_1} + \underbrace{\nu u G}_{V_2}. \tag{2.10}$$

Here LA is the local acceleration, CV the convection term and PG the pressure gradient term and V_1 and V_2 are the viscous terms. An interesting observation is that formally (2.10) is similar to the one-dimensional Burgers equation except for the pressure gradient term and part of the viscous terms.

2.3. *Kinetic energy balance*

The turbulent kinetic energy is defined as $k = \boldsymbol{v}\cdot\boldsymbol{v}/2 = u^2/2$. Multiplying both sides of (2.10) with u, one obtains

$$u\frac{\partial u}{\partial t} + u^2\frac{\partial u}{\partial s} = -u\frac{\partial p}{\partial s} + \nu u\nabla^2 u + \nu u^2 G. \tag{2.11}$$

From the relation

$$u\nabla^2 u = \frac{1}{2}\nabla^2(u^2) - \nabla u\cdot\nabla u \tag{2.12}$$

and the definition of the shape factor G in (2.9), it yields

$$\underbrace{\frac{\partial k}{\partial t}}_{LA_k} + \underbrace{u\frac{\partial k}{\partial s}}_{CV_k} = \underbrace{-u\frac{1}{\rho}\frac{\partial p}{\partial s}}_{PG_k} + \underbrace{\frac{\nu}{2}\nabla^2(u^2)}_{V_{1k}} - \underbrace{\nu(\nabla u\cdot\nabla u - u^2 G)}_{V_{2k}} \tag{2.13}$$

Similar to (2.10), here LA_k, CV_k, PG_k, V_{1k} and V_{2k} represent the the local acceleration, the convection, the pressure gradient and the viscous terms for k, respectively. In (2.13), V_{2k} is positive definite, corresponding the energy dissipation ε:

$$\varepsilon \equiv \nu(\nabla u\cdot\nabla u - Gu^2) = \nu(\nabla u\cdot\nabla u - 2kG). \tag{2.14}$$

Equation (2.14) suggests that energy dissipation ε consists of two parts: one is the square of the gradient of u, which is not only from the stretching along the streamline direction but also from the variation of u in other directions; another part is the multiplication of the kinetic energy k with the shape factor G. Therefore it seems that the kinetic energy itself can also play an explicit role in determining the energy dissipation ε. In addition, different from the Cartesian coordinate, the fact that different material points along streamlines have various volume-weighting factors should be taken into account to calculate the mean ε in space.

3. Numerical evaluation from DNS

To estimate the magnitudes of different terms in the balance equations, two DNS cases have been performed for homogeneous shear turbulence with an imposed velocity gradient $S = \mathrm{d}u_1/\mathrm{d}x_2$ in a 2π cubic domain, as shown in figure 4. A spectral method was used to perform spatial derivatives in the Navier–Stokes equations, and a third-order Runge–Kutta scheme was used for time advancement. The continuity equation was satisfied by rewriting the convection terms into a skew-symmetric form.

	Case 1	Case 2
Mean shear $S = \mathrm{d}\langle v_1 \rangle / \mathrm{d}x_2$	1.5	1.5
Grid points	512^3	2048^3
Viscosity ν	0.003	0.0009
Turbulent kinetic energy k	2.609	3.089
Dissipation ε	0.974	1.080
Kolmogorov scale η	0.0129	0.00510
Taylor scale λ	0.284	0.160
$Re_\lambda = v_{rms}\lambda/\nu$	125.0	255.0
Resolution $\Delta x/\eta$	0.95	0.62

TABLE 1. Characteristic parameters of DNS.

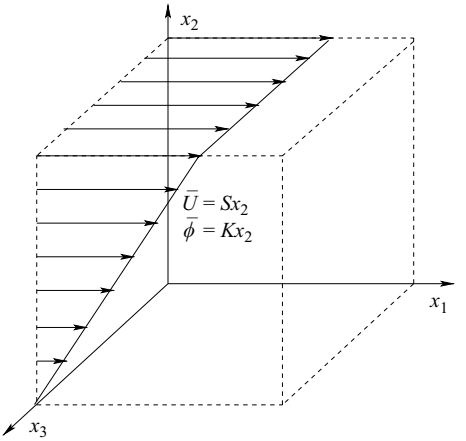

FIGURE 4. The flow configuration of homogeneous shear turbulence. The mean velocity gradient S and the scalar gradient K are the input parameters. The governing equations are solved in a moving grid attached with the mean flow.

To ensure a high enough resolution to discern fine structures numerically, the grid size Δx needs to be smaller than the Kolmogorov scale η. The main characteristic parameters of the simulations are listed in Table 1. For more details of the numerical algorithm, the readers are refereed to the relevant work (Wang 2008).

3.1. *Streamline segment and streamtube segment*

As has been discussed, usually a streamline from any grid point may be infinitely long if no stagnation point can be hit. The concept of the streamline segment is used to partition streamlines according to some natural topology. Starting from each grid point, a streamline can be uniquely traced until the local maximal u_{max} and the local minimal u_{min} are reached. The segment bounded by two extremal points is defined as the streamline segment of the given grid point, and the arclength l between these two extrema is the length of this segment. Specifically, a segment is termed positive if it points from u_{min} to u_{max} and negative if it points from u_{max} to u_{min}.

The streamline segment idea contributes a well-defined length scale, based on which further quantitative analyses become possible by grouping the grid points according to their segment lengths. Mathematically streamlines are not a volumetrical topology, which then is of less physical importance and interest for further applications. Therefore an extended concept, namely the streamtube segment, has been put forward.

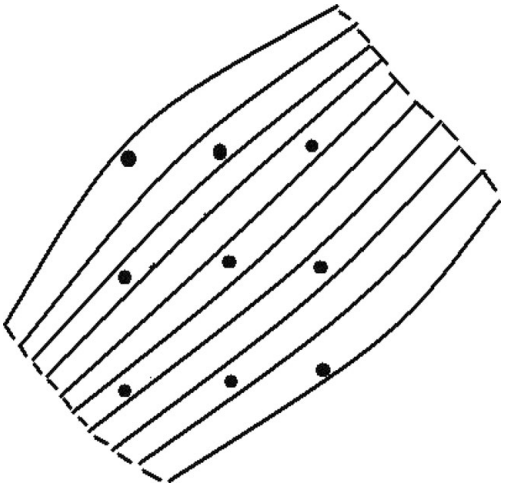

FIGURE 5. The schematic explanation of the streamtube segments. From each grid point (solid dot) in a homogeneous point array, a streamtube encompassing the streamline segment can be configured. All of the streamtube segments are organized in a non-overlapping and space-filling manner.

As shown in the schematic in figure 5, from each grid point in a homogeneous point array, the streamline segment passing through can be determined. Streamtubes encompassing the segments can be configured in such a way that all of the streamtube segments are non-overlapping and space filling. It is obvious that the boundaries of the individual streamtube segments are not determined; however, theoretically by volume-weighting average, the final statistical results will be independent of the boundary demarcation. In this sense, the streamtube segment partition provides us a space-filling structure to analyse the vector fields following the intrinsic topology of vectors. Thus potentially we can apply (1.1) to reconstruct vector-related properties by volume-weighting all the streamtube segments. Because a segment volume is proportional to the number of homogeneously distributed grid points which this segment can encompass, numerically the volume-weighting average of the streamtube segments is equivalent to the average of the streamline segments from all grid points. This argument needs to be taken into account hereinafter.

3.2. *Galilean invariance*

Because streamlines depend on the flow velocity, in different reference frames the flow velocity varies, which implies that streamlines are not Galilean invariant. This point can be illustrated by calculating $\langle \boldsymbol{n} \rangle$, the mean of the orientation vector $\boldsymbol{n}$, which is defined as the unit vector pointing from the maximal (minimal) to the minimal (maximal) point of each negative (positive) segment. For DNS case 1, $\langle \boldsymbol{n} \rangle$ has been evaluated in two different reference frames:

(i) $\langle \boldsymbol{n} \rangle = [4.88\times10^{-4},\ -6.28\times10^{-4},\ -3.69\times10^{-3}]$, when the translation velocity is $[0, 0, 0]$;

(ii) $\langle \boldsymbol{n} \rangle = [0.345,\ 3.3\times10^{-2},\ -9.08\times10^{-3}]$, when the translation velocity is $[1, 0, 0]$.

Although the flow fields can be partitioned differently in different reference frames, any parameter after volume-weighting average remains the same because of the same spatial domain. In other words, Galilean invariance does not introduce any effect on the final statistics averaged for the whole grid points. Usually for turbulence, the frame in which the mean flow is zero is of special interest, and it will work as the

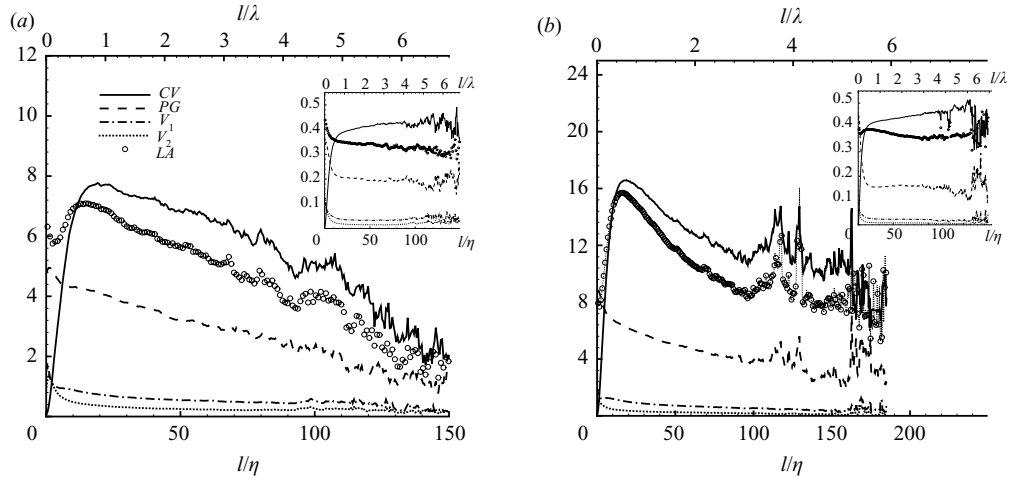

FIGURE 6. The absolute value of LA, CV, PG, V_1 and V_2 in (2.10) for (a) case 1 and (b) case 2. The insets show the relative magnitudes of these terms.

default reference frame to define streamlines in this context. A similar consideration appears in the study of stagnation points as well (Chen, Goto & Vassilicos 2006).

3.3. *Numerical results*

Numerically the streamline segments can be determined by computing the sign of the velocity stretching rate $\boldsymbol{t}\cdot\nabla\boldsymbol{v}\cdot\boldsymbol{t}$ along streamlines. It is obvious that this stretching rate changes sign, either from positive to negative or from negative to positive, when it crosses an extremal point. Compared with other methods, this criterion was found to be robust with a better numerical accuracy.

For the classical statistical tools, length scales are chosen from two arbitrary spatial points. Very differently, by introducing the streamline segments length scales can uniquely be defined. With respect to the new scales, DNS results of (2.10) for cases 1 and 2 are plotted in figures 6(a) and 6(b), respectively, in which the insets show the relative magnitudes of these terms. By comparing case 1 and case 2, it can be seen that the magnitudes of these terms are very different, and this tendency becomes stronger when the Reynolds number is larger. According to the results by Monin & Yaglom (1975) and Lin (1953), the total acceleration of fluid particles is largely dominated by the irrotational part, i.e. the pressure gradient, while the solenoidal viscous part is very small, especially for high-Reynolds-number turbulence. The same conclusion has also been drawn from the numerical verification by Vedula & Yeung (1999) and Tsinober, Vedulab & Yeung (2001). Generally for large Reynolds numbers, the relative magnitudes of the terms in (2.10) are

$$LA \sim CV \gg PG \gg V_1 \gg V_2. \tag{3.1}$$

Similarly, the terms in (2.13) are shown in figure 7. Comparison of the tendencies of both DNS cases suggests that relation (3.1), which is valid for the momentum balance, holds for the kinetic energy balance as well at large Reynolds numbers, i.e.

$$LA_k \sim CV_k \gg PG_k \gg V_{1k} \gg V_{2k}. \tag{3.2}$$

Figure 7 indicates that the magnitude of ε is very small, while as we know, ε is the only sink to balance the energy input at large scales. Thus the net effect of other

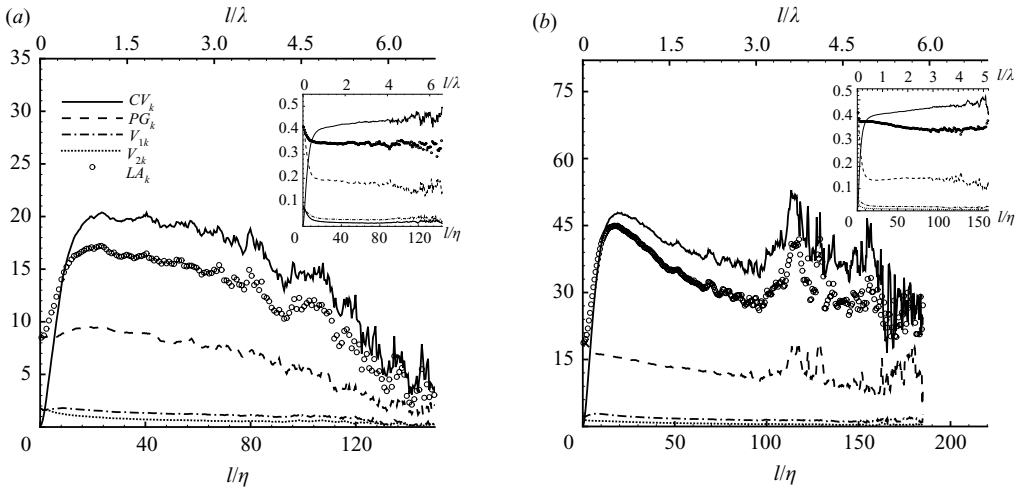

FIGURE 7. The absolute value of LA_k, CV_k, PG_k, V_{1k} and V_{2k} in (2.13) for (*a*) case 1 and (*b*) case 2. The insets show the relative magnitudes.

terms in (2.13) must be very weak, which can be explained by the counteraction of large positive and negative fluctuations.

The equations in the streamline coordinate discussed above appear different from what they are in the Cartesian coordinate. One advantage of the curvilinear frame is its dimensional independence; i.e. these equations in scalar form remain unchanged in different dimensional spaces.

4. Geometrical properties

Figure 8 shows the variation of u along several arbitrarily picked streamline samples a, b and c. It can be seen that the negative segments generally are steeper than the positive segments.

In characterizing the shapes of the streamline segments, the two most important parameters are the arclength l and the difference of the velocity magnitude, i.e. $\Delta u = u_{max} - u_{min}$ for the positive segments and $\Delta u = u_{min} - u_{max}$ for the negative segments, with the consideration that the streamline segments are always along the velocity vector directions. The numerical result from DNS case 1 of the joint p.d.f. $P(\Delta u, l)$ is shown in figure 9. The similar result for case 2 is omitted here. The most obvious feature of this joint p.d.f. is its non-symmetry: the negative part ($\Delta u < 0$) extends over a smaller range of l, while the positive part ($\Delta u > 0$) is relatively longer. The dependence of Δu on l suggests that on average the longer streamline segments have larger velocity differences. The two solid lines in figure 9 are the conditional means of the positive and negative parts. It is clear that the mean slope ($\sim$3.9) of the negative part is larger than that ($\sim$2.9) of the positive part. The subplot at the upper left-hand side is a local enlargement to show finer structures.

In fact the non-symmetry of $P(\Delta u, l)$ is naturally a kinematic outcome. Considering a positive segment, the strain rate along thus is positive (extensive) because of a positive Δu, which will extend this segment and make it longer, while for a negative segment with $\Delta u < 0$, the length will be reduced under the action of a compressive strain. Consequently one may expect that on average the positive segments are longer and the negative segments are shorter. By the same argument, it is also reasonable to conclude that the volume occupied by the positive segments must be larger than

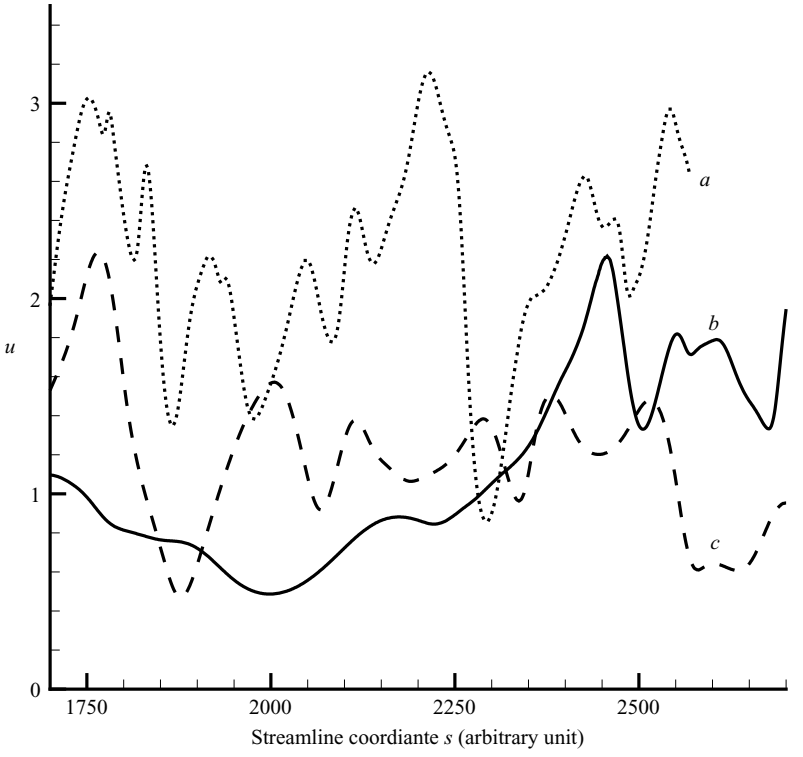

FIGURE 8. The variation of u along individual streamline samples. It can be observed that on average the negative segments are steeper than the positive ones.

the negative part, which can be verified numerically; for instance, for DNS case 2 the volume ratio between the positive and negative segments is about 1.3:1.

From the joint p.d.f., the marginal p.d.f.s of l, separately plotted for the positive and negative parts for cases 1 and 2, are shown in figure 10. It can be seen that for both cases, although the mean values of the positive and negative groups differ much, the two p.d.f.s reach the maxima at almost the same location, after which the p.d.f. of the negative group decreases faster. Comparing case 2 with case 1, the decaying part ($l/\eta > 20$) fits better to an exponential tail at higher Re. It is reasonable to expect shorter streamline segments on average at higher Reynolds numbers. DNS results for case 1 show that the mean lengths of the positive and negative segments are 0.319 and 0.255, respectively, while these numbers for case 2 are 0.136 and 0.105, respectively. Furthermore, the relative difference between the length of positive and negative parts increases for larger Reynolds numbers, $(0.319 - 0.255)/0.319 = 0.20$ while $(0.136 - 0.105)/0.136 = 0.29$, which may indicate that the more intensive turbulent motion can strengthen the difference between the positive and negative segments.

Phenomenologically, extremal points are generated by turbulent perturbations. At the same time, fluid viscosity is responsible for smearing away the fluctuation of u to produce longer segments, similar to the evolution of gradient trajectories (Wang & Peters 2006). An analytical description of the length variation of the streamline segments will be the subject of further research.

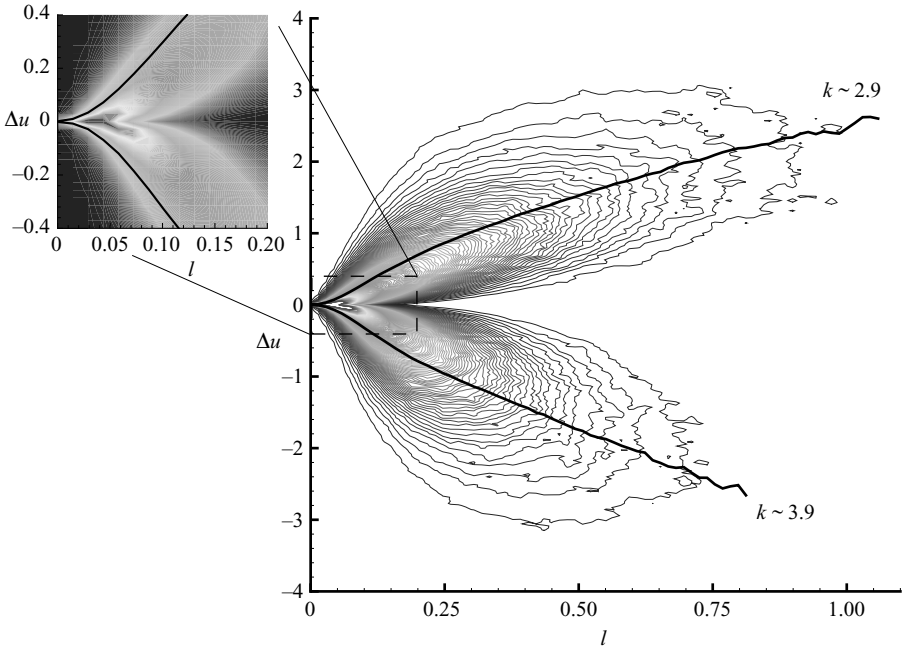

FIGURE 9. The joint p.d.f. of the velocity difference and the arclength of the streamline segments. The solid lines are the conditional means for the positive and negative parts correspondingly. The subplot at the upper left-hand side is a local enlargement to show finer structures.

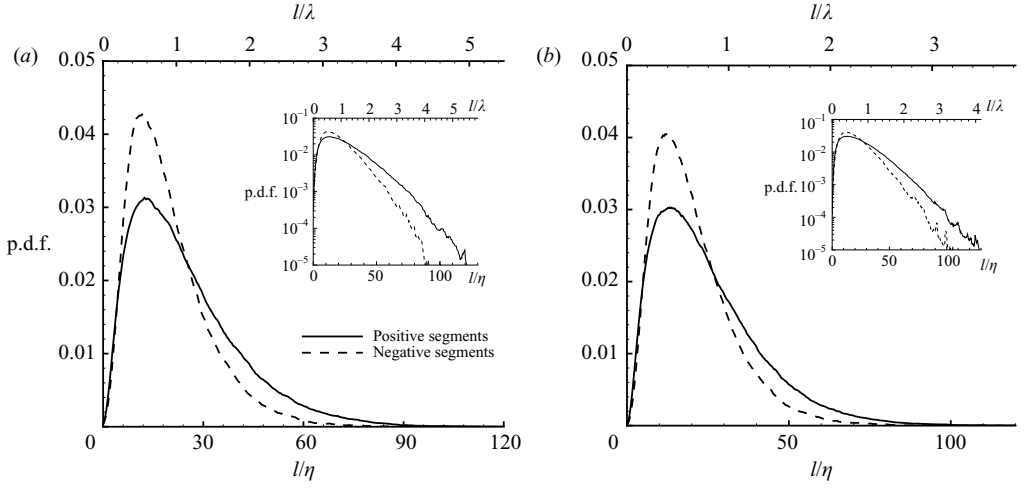

FIGURE 10. The p.d.f. of the length distribution of the positive and negative streamline segments for (*a*) case 1 and (*b*) case 2.

4.1. *On the skewness of the velocity derivative*

Skewness, one of the essential issues in turbulence research, is closely related to other important properties such as intermittency and anisotropy. The skewness of the velocity derivative along x direction in the Cartesian frame can quantitatively be

measured by

$$S = \langle(\partial v_1/\partial x)^3\rangle/\langle(\partial v_1/\partial x)^2\rangle^{3/2}; \tag{4.1}$$

S is negative for various turbulent flows at different Reynolds numbers (Sreenivasan & Antonia 1997). In analysing the balance equation of turbulent enstrophy, Taylor (1938) argued intuitively that the production of enstrophy should be positive because when positive extension of a vortex filament occurs, the magnitude of the local vorticity increases because of the consequent lateral contraction and angular acceleration. This observation is consistent with the general tendency in turbulent motion for points to move apart and for lines to lengthen, giving a tendency for the average value of enstrophy to increase. Batchelor & Townsend (1947) derived that the production term in the enstrophy equation is directly proportional to skewness, as defined in (4.1); thus the negativeness of skewness based on the observation by Taylor can be demonstrated, but this explanation is speculative and by far not satisfying.

In the context of streamline segments and the non-symmetry of $P(\Delta u, l)$, the negative skewness is naturally a kinematic outcome. For isotropic turbulence, it is plausible to expect that the streamline segments (along the positive u direction) are non-preferentially orientated. It is easy to verify that for a straight positive streamline segment, its contribution to skewness in the Cartesian coordinate system must be positive, no matter whether it is along x or $-x$ direction, while the skewness of a straight negative streamline segment must be negative, no matter which direction it points to, which means that the contribution to skewness from chaotically orientated streamline segments cannot counteract. To investigate the skewness of the positive and negative segments separately, both DNS cases have been analysed. Specifically we have the following.

(i) Case 1: 0.060 from positive segments; -0.49 from negative segments.

(ii) Case 2: 0.104 from positive segments; -0.612 from negative segments.

Because on average the (absolute value of) slope of the negative segments are larger than that of the positive segments, the negative part in S is significantly amplified to lead to negative skewness. The definition in (4.1) can be understood as the average skewness of streamline segments projected in x direction. For the higher-Reynolds-number case, case 2, both the positive and negative contributions become larger because of a stronger extension or compression of the streamline segment. Overall their difference must be larger as well, which may shed light on the observation that skewness increases weakly with the Reynolds number (Sreenivasan & Antonia 1997).

The above kinematic or geometrical explanation of the negativeness of skewness holds in any dimensional spaces, while the arguments by Taylor (1938) may only fit to three-dimensional cases. There are some issues in the discussion of the two-dimensional skewness as well. In the modelling based on the one-dimensional Burgers equation by Li & Meneveau (2006), the negative skewness can be well understood because of the nonlinear term to steepen the velocity gradient. Because the model of the velocity gradient tensor is space dimension dependent, which is from the effect of mass conservation, it has been argued that the so-called self-cancellation mechanism prevents the growth of negative skewness and intermittency in two-dimensional space. It is true that in two-dimensional space skewness is much weaker than in higher-dimensional cases because of the constraint of the continuity equation; however, from the present kinematic viewpoint, the negativeness of skewness can never be prohibited because of the non-symmetry induced by the stretching strain and compressive strain even in two-dimensional space. In fact, in the work by Boffetta, Celani & Vegassola (2000), quantitative evidences have showed

that although negative skewness in two-dimensional turbulence is largely suppressed, the deviation from Gaussianity does exist, which can more easily be amplified if even higher odd-order ($\geqslant 5$) structure functions are considered.

Phenomenologically intermittency and anisotropy are intimately related to each other (Warhaft 2000). It has been clarified many times that scalar fluctuations, at whichever scale, are always anisotropic, in violation of the generally accepted return-to-isotropy picture. Similarly from the structure of the streamline segments, the respective action by stretching and compressive strain on the positive and negative streamline segments, even at the smallest scales, does not disappear; yet the corresponding characteristic time of the strain at small scales is smaller to make the difference between the positive and negative segments, and thus anisotropy, weaker.

5. Dynamical properties

Compared with the geometrical topology, which is considered from the kinematic viewpoint, to understand the dynamic effect of turbulence on the streamline segments is another key aspect. The important parameters, pressure and kinetic energy dissipation, are investigated in this section.

5.1. *Pressure*

Perhaps the understanding of pressure is one of the most controversial fields in turbulence, with regard to the scaling of structure functions, the characteristic length of the pressure gradient and the like (George & Beuther 1984; Gotoh & Rogallo 1999; Gotoh & Fukayama 2001). For incompressible flows, the Poisson equation for pressure,

$$\nabla^2 p = \left(\frac{1}{2}\omega^2 - s^2\right)\rho, \tag{5.1}$$

is a non-local function of the velocity field, where the enstrophy $\omega^2 = \omega_i\omega_i$, $\omega_i \equiv \epsilon_{ijk}\partial_j v_k$ and $s^2 = S_{ij}S_{ij}$, $S_{ij} \equiv (\partial_j v_i + \partial_i v_j)/2$. Equation (5.1) indicates that pressure has a strong correlation with vorticity: regions with high vorticity and low strain rates are sources of low pressure, while low vorticity and high strain rates are responsible for high pressure. Robinson (1991) argued that most low-pressure regions are elongated and correspond to vortex cores; high-pressure regions occur usually when high-speed fluid impacts low-speed fluid, thus forming a convecting stagnation point. Because of the inconvenience in improving experimental accuracy, detailed study of pressure became possible after the performance of high-resolution DNS. From DNS case 1 the interaction of low-pressure isosurfaces (red sheets) and vortex tubes (light blue) is shown in figure 11. It is obvious that quite probably these two structures overlap; however, low-pressure isosurfaces are to some extent sheet-like, not as slender as vortex tubes. Therefore it may be expect that regions with high vorticity may also have high strain rate, which then excludes low pressure. The DNS results for decaying isotropic turbulence (Kalelkar 2006) show the same sheet-like structure, especially at low Reynolds numbers; only at the fully decayed stage, low-pressure isosurfaces may evolve to slender and more fractal pieces.

In addition, for incompressible flows, the following relation holds (Rotta 1972):

$$\overline{\boldsymbol{v}\cdot\nabla p} = \overline{\nabla\cdot(p\boldsymbol{v})} - \overline{p\nabla\cdot\boldsymbol{v}} = 0. \tag{5.2}$$

This overall relation (5.2) is not capable of investigating further the orientation between the pressure gradient ∇p and the velocity vector $\boldsymbol{t}$: if they are uncorrelated

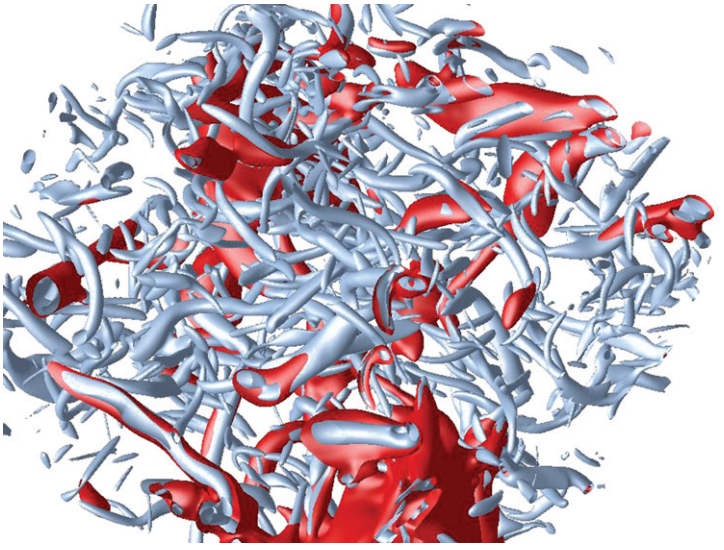

FIGURE 11. The interaction of low-pressure isosurfaces (red sheets) and vortex tubes (light blue) from DNS case 1.

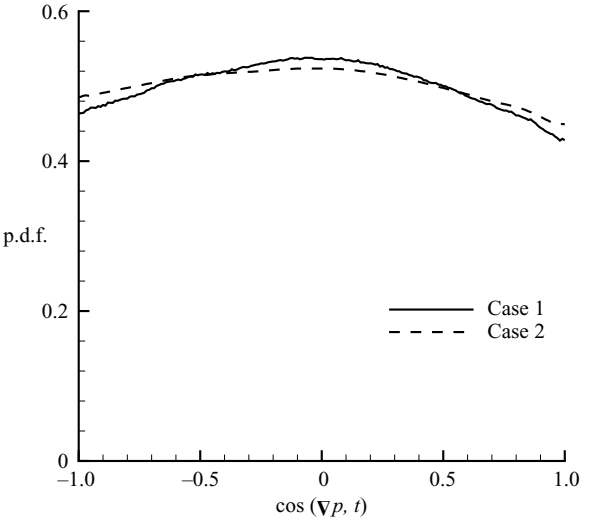

FIGURE 12. The p.d.f. of the cosine between the pressure gradient and the velocity vector.

or most probably will be perpendicular? For DNS cases 1 and 2 the p.d.f.s of $\cos(\nabla p, \boldsymbol{t})$, the cosine between ∇p and $\boldsymbol{t}$, are shown in figure 12. The symmetry of the p.d.f.s is consistent with the zero statistical average of $\overline{\boldsymbol{v} \cdot \nabla p}$ in (5.2). In addition, both p.d.f.s reach the maximal at $\cos(\nabla p, \boldsymbol{t}) = 0$; however, they are quite flat without much variation, especially for the higher-Reynolds-number case, case 2, which indicates that ∇p and $\boldsymbol{t}$ are almost uncorrelated at higher Reynolds numbers.

By studying the positive and negative segments separately, some finer structures can be viewed. Figure 13(a) shows for both DNS cases similar results as figure 12, but separately for the positive and negative segments (in this sense, figure 12 is a

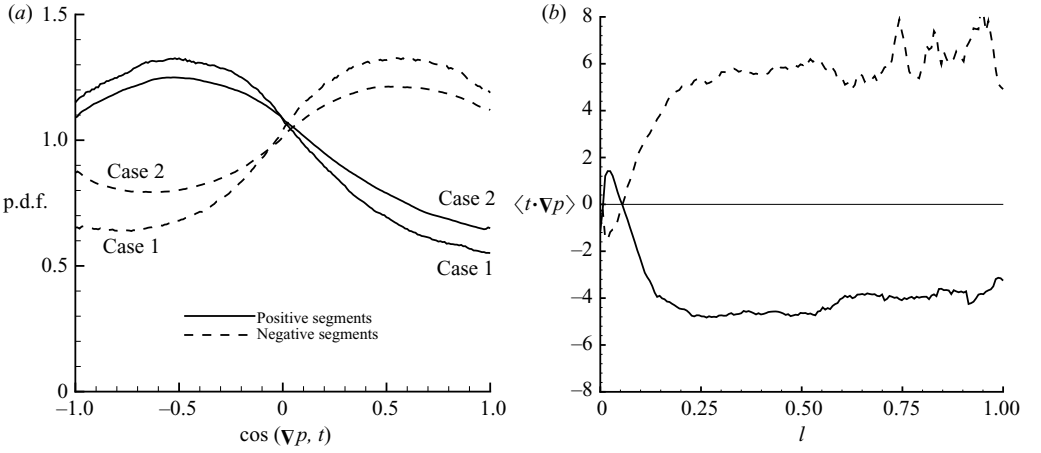

FIGURE 13. Separately for the positive and negative segments, the orientation between the pressure gradient and the velocity vector: (*a*) the p.d.f. of the cosine angle for both DNS cases; (*b*) the conditional mean of $\overline{\boldsymbol{t}\cdot\nabla p}$ with reference to the segment length for DNS case 1.

resultant one). Differently, the p.d.f.s here are not symmetrical any more. Instead, the p.d.f. for the positive segments is left inclined, i.e. the pressure gradient tends to align opposite to the velocity vector to decelerate the fluid, while for the negative group it is right inclined, i.e. the pressure gradient is likely to align with the velocity vector to accelerate the fluid. Therefore, the overall effect of the pressure gradient is to 'shift' kinetic energy from the positive segments to the negative segments. For the larger-Reynolds-number case, case 2, its two p.d.f.s become flatter, which means the pressure gradient tends to be more chaotical and less correlated with the velocity vector. Following the same mechanism, from figure 13(*b*) (for case 1) one can see that on average $\overline{\boldsymbol{t}\cdot\nabla p}$ is negative for the positive segments, while it is positive for the negative segments, except for small segments ($l < 0.05$). The reason for this inverse tendency may be ascribed to the viscosity effect, which is more predominant at small scales.

5.2. *Kinetic energy dissipation*

The kinetic energy dissipation ε is a key quantity in turbulence dynamics. For a better understanding of this parameter defined as (2.14) along streamlines, it is meaningful to analyse the dependence of ε on the normalized coordinate s^*, which is the ratio of the arclength between a given grid point and the starting point of its streamline segment (u_{min} for the positive segments and u_{max} for the negative segments) to the total segment arclength. Figure 14 shows the results for three subgroups: $0 < l/l_m < 0.5$, $1.0 < l/l_m < 1.5$ and $2.5 < l/l_m$, representing small (group 1), intermediate (group 2) and large (group 3) streamline segments, respectively, where l_m is the overall mean of l. It can be seen that $\langle\varepsilon\rangle$, the overall mean ε, is almost the same for the positive and negative segments, which suggests that statistically the sign of strain along streamlines may not dominate ε.

Furthermore, figures 14(*a*) and 14(*b*) show the following relation for both the positive and negative streamline segments:

$$\langle\varepsilon\rangle_{group1} > \langle\varepsilon\rangle_{group2} > \langle\varepsilon\rangle_{group3}. \tag{5.3}$$

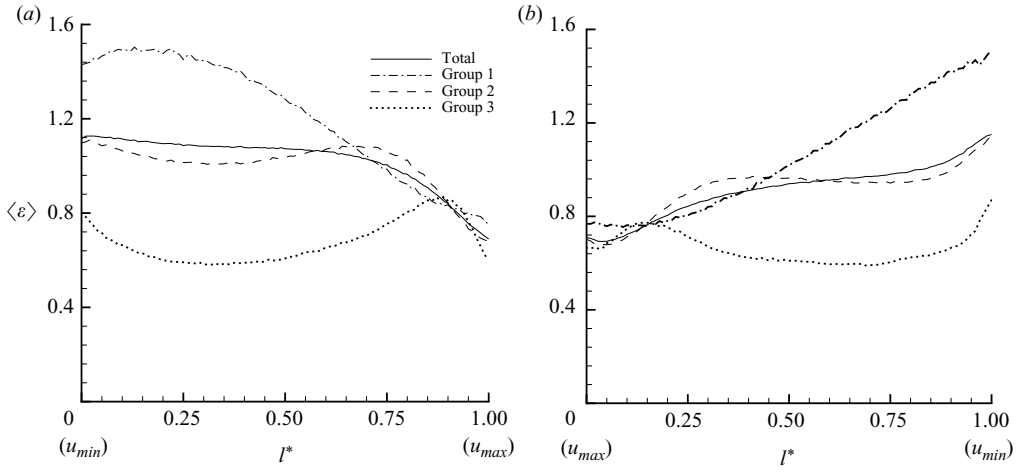

FIGURE 14. Numerical results for DNS case 1 of the variation of ε with respect to s^* for different subgroups of (a) the positive segments and (b) the negative segments.

From the energy cascade picture, it has been agreed that small scales generally are highly responsible for large ε. Because of the random motion in turbulence, larger eddies can squeeze each other into highly deformed regions. However, here the concept of 'turbulent eddy' is illustrative and descriptive rather than quantitative. Streamline segment analysis provides us a clear view to mark the size of eddies in a precise manner. It is reasonable to expect that the cliff regions should very probably be filled by small streamline segments.

It is interesting to note that for group 1, comprised of small segments, regions around u_{min} ($s^* = 0$ for positive and $s^* = 1$ for negative segments) have much larger $\langle\varepsilon\rangle$ than those around u_{max} ($s^* = 1$ for positive and $s^* = 0$ for negative segments), while for intermediate (group 2) and large segments (group 3), this difference becomes much weaker or almost disappears. Mathematically from the expression of ε in (2.14), there are two contributions, $\nu\nabla u\cdot\nabla u$ and $-2\nu kG$. For regions around extremal points for short streamline segments, that $\partial u/\partial s$ is close to zero makes it plausible to expect a small ∇u and $\nu\nabla u\cdot\nabla u$ as well. Considering the second part, i.e. $-2\nu kG$, for short segments k may not differ much at u_{max} and u_{min} because of the close location. Therefore the shape factor G needs to have a large difference between regions around u_{max} and u_{min} to lead to a large difference of ε. As has been mentioned, G is a function of the geometrical topology of stream lines, for instance the curvature and the torsion. It has been shown (Braun, Lillo & Eckhardt 2006) that there is some correlation between ε and the curvature of Lagrangian particles. Further relations among these factors and ε with respect to the streamline segments are important and meaningful to explore.

6. Concluding remarks

The present paper has concentrated mainly on the dynamics and geometrical structures of turbulent flows based on streamline analysis. On the one hand, turbulent flows are disorganized because of the random motion of turbulent eddies; on the

other hand, the organized parts assume important spatial structures. By analysing streamlines, turbulent structures may quantitatively be described.

Starting from each grid point, its streamline can be traced by following the local velocity vectors. According to the velocity magnitude u along the streamline, a local maximal u point and a local minimal u point can de determined as well. The part of the streamline bounded by two adjacent extremal points is defined as the streamline segment (of the grid point). Because of mass conservation, extremal surfaces, which consist of extremal points (either maximal or minimal), have zero Gaussian curvature. In two-dimensional space, extremal surfaces degenerate to straight lines, which can only be redirected or broken by stagnation points or by the boundaries of flow fields.

The importance of space filling has been addressed in dissipation element analysis for the scalar fields (Wang & Peters 2006, 2008). For the vector fields, the streamline segments can be physically extended into the streamtube segments, which are space filling as well. This new structure allows for new insights into vector-related statistics in turbulence, as described by (1.1). Statistics based on streamtube segment analysis need to be weighted by the volume of tube segments. Because a segment volume is proportional to the number of homogeneously distributed grid points which this segment can encompass, numerically volume-weighting average of the streamtube segments is equivalent to the average of the streamline segments from all grid points. This new structure, together with the transformed basic equations along streamlines, may shed light on understanding turbulence in a more quantitative and precise manner.

Depending on the variation of the velocity magnitude, the streamline segments can further be subgrouped into positive and negative segments. The statistics of the positive segments and the negative segments behave differently. The overall properties are the resultants from these two subgroups. Kinematically the positive segments are inclined to be stretched, while the negative segments are compressed; therefore on average the positive segments are longer than the negative segments. This explains naturally the negative skewness of the velocity derivative.

Furthermore, along the streamline segments the conditional mean of kinetic energy dissipation and the interaction between the pressure gradients and the velocity vectors appear different from that in the Cartesian frame. The orientation between the pressure gradient and the velocity vector determines the turbulent dynamics. Statistically these two vectors do not align; however, the finer structures separately from the positive and negative segments show a strong alignment, indicating some footprint of laminar flows in turbulence. For streamline segments with different sizes the kinetic energy dissipation ε has different properties. On average small segments are highly responsible for large energy dissipation. Especially the shape factor plays a critical role in determining the local dissipation. Moreover, ε in regions around local minimal u is much larger than those around local maximal u. For larger segments, the difference becomes much weaker.

This work is funded by Deutsche Forschungsgemeinschaft under grant Pe 241/38-1. The encouragement and enlightening suggestions from Prof. N. Peters (RWTH-Aachen) are greatly appreciated. The helpful discussion with Dr J. P. Mellado (RWTH-Aachen) was of great importance in shaping this paper. The necessary guidance from Professor C. Tong (Clemson University) has improved this work much. The author acknowledges the Juelich Supercomputing Centre, Germany, for access to the Bluegene supercomputer for calculation.

REFERENCES

Aivazis, K. A. & Pullin, D. I. 2001 On velocity structure functions and the spherical vortex model for isotropic turbulence. *Phys. Fluids* **13** (7), 2019–2029.

Batchelor, G. K. & Townsend, A. A. 1947 Decay of vorticity in isotropic turbulence. *Proc. R. Soc.* A **190**, 534–550.

Boffetta, G., Celani, A. & Vegassola, M. 2000 Inverse energy cascade in two-dimensional turbulence: deviations from Gaussian behaviour. *Phys. Rev.* E **61** (1), 29–32.

Braun, W., Lillo, F. D. & Eckhardt, B. 2006 Geometry of particle paths in turbulent flows. *J. Turbul.* **7** (62), 1–10.

Brons, M. 2007 Streamline topology: patterns in fluid flows and their bifurcations. *Adv. Appl. Mech.* **41**, 1C43.

Chen, L., Goto, S. & Vassilicos, J. C. 2006 Turbulent clustering of stagnation points and inertial particles. *J. Fluid Mech.* **553**, 143C154.

Davey, A. 1961 Boundary-layer flow at a saddle point of attachment. *J. Fluid Mech.* **10**, 593–610.

Davila, J. & Vassilicos, J. C. 2003 Richard's pair diffusion and the stagnation point structure of turbulence. *Phys. Rev. Lett.* **91** (14), 144501.

George, W. K., Beuther, P. D. & Arndt, R. E. A. 1984 Pressure spectra in turbulent free shear flows. *J. Fluid Mech.* **148**, 155–191.

Gotoh, T. & Fukayama, D. 2001 Pressure spectrum in homogeneous turbulence. *Phys. Rev. Lett.* **86** (17), 3775–3778.

Gotoh, T. & Rogallo, R. 1999 Intermittency and scaling of pressure at small scales in forced isotropic turbulence. *J. Fluid Mech.* **396**, 257–285.

Hamman, C., Klewicki, J. & Kirby, R. 2008 On the Lamb vector divergence in Navier–Stokes flows. *J. Fluid Mech* **610**, 261–284.

Kalelkar, C. 2006 Statistics of pressure fluctuations in decaying isotropic turbulence. *Phys. Rev.* E **73**, 046301.

Kaneda, Y. & Ishihara, T. 2006 High-resolution direct numerical simulation of turbulence. *J. Turbul.* **7** (20), 1–17.

Li, Y. & Meneveau, C. 2006 Intermittency trends and Lagrangian evolution of non-Gaussian statistics in turbulent flow and scalar transport. *J. Fluid Mech.* **558**, 133–142.

Lighthill, M. J. 1963 Attachment and separation in three-dimensional flow. *Laminar Boundary Layers* (ed. L. Rosenhead). **2.6**, 72–82. Oxford University Press.

Lin, C. C. 1953 On Taylor's hypothesis and the acceleration terms in the Navier–Stokes equations. *Quart. Appl. Math.* **10**, 295–306.

Lumley, J. L. & Yaglom, A. M. 2001 A century of turbulence. *Flow Turbul. Combust.* **66**, 241–286.

Mellado, J. P., Wang, L. & Peters, N. 2009 Gradient trajectory analysis of a scalar field with external intermittency. *J. Fluid Mech.* **626**, 333–365.

Moffatt, H. K., Kida, S. & Ohkitain, K. 1994 Stretched vortices: the sinews of turbulence; large-Reynolds-number asymptotics. *J. Fluid Mech.* **259**, 241–264.

Moffatt, H. K. & Tsinober, A. 1992 Helicity in laminar and turbulent flow. *Annu. Rev. Fluid Mech.* **24**, 281–312.

Monin, A. S. & Yaglom, A. M. 1975 *Statistical Fluid Mechanics: Mechanics of Turbulence*, vol. 2. MIT Press.

Perry, A. E. & Chong, M. S. 1987 A description of eddying motions and flow patterns using critical-point concepts. *Annu. Rev. Fluid Mech.* **19**, 125–155.

Petrila, T. & Trif, D. 2005 *Basics of Fluid Mechanics and Introduction to Computational Fluid Dynamics.* Springer.

Rao, P. 1978 Geometry of streamlines in fluid flow theory. *Def. Sci. J.* **28** (4), 175–178.

Robinson, S. K. 1991 Coherent motions in the turbulent boundary layer. *Annu. Rev. Fluid Mech.* **23**, 601–39.

Rotta, J. C. 1972 *Turbulente Strömungen.* B. G. Teubner Stuttgart.

She, Z. S., Jackson, E & Orszag, S. A. 1990 Intermittent vortex structures in homogeneous isotropic turbulence. *Nature* **344**, 226–228.

Sreenivasan, K. R. & Antonia, R. A. 1997 The phenomenology of small-scale turbulence. *Annu. Rev. Fluid Mech.* **29**, 435C72.

Synge, J. L. & Lin, C. C. 1943 On a statistical model of isotropic turbulence. *Trans. R. Soc. Can.* **37**, 45–79.

Taylor, G. I. 1938 Production and dissipation of vorticity in a turbulent fluid. *Proc. R. Soc.* A **164**, 15–23.

Tsinober, A., Vedulab, P. & Yeung, P. K. 2001 Random Taylor hypothesis and the behaviour of local and convective accelerations in isotropic turbulence. *Phys. Fluids* **13**, 1974–1984.

Vedula, P. & Yeung, P. K. 1999 Similarity scaling of acceleration and pressure statistics in numerical simulations of isotropic turbulence. *Phys. Fluids* **11** (5), 1208–1220.

Wang, L. & Peters, N. 2006 The length-scale distribution function of the distance between extremal points in passive scalar turbulence. *J. Fluid Mech.* **554**, 457–475.

Wang, L. & Peters, N. 2008 Length-scale distribution functions and conditional means for various fields in turbulence. *J. Fluid Mech.* **608**, 113–138.

Wang, L. 2008 Geometrical description of homogeneous shear turbulencce using dissipation element analysis. PhD thesis, Shaker, Germany.

Warhaft, Z. 2000 Passive scalars in turbulent flows. *Annu. Rev. Fluid Mech.* **32**, 203–40.

Yannacopoulos, A. N., Rowlands, G. & King, G. P. 2002 A Melnikov function for the breakup of closed streamlines in steady Navier–Stokes flows. *Phys. Fluids* **14** (5), 1572–1579.